JCSE The Journal of Corrosion Science and Engineering

21st Century Corrosion Science

Volume 6 Paper C111

Effect of Magnetic Fields on Corrosion

Y. C. Tang, M. Gonzalez-Torreira, S. Yang, A. J. Davenport

Metallurgy and Materials, School of Engineering, The University of Birmingham, Edgabston, Birmingham B15 2TT, UK.
a.davenport@bham.ac.uk

Abstract

The effect of magnetic fields on corrosion processes was investigated. The Lorenz force was found to cause solution flow for corrosion of NdFeB magnets under drops of HCl, and copper sheet under drops of nitric acid when a small magnet was attached to the back of the sheet. The field generated by a PrFeB magnet also influenced the morphology of attack by nitric acid. In experiments with artificial pits grown by dissolution of wires encapsulated in epoxy resin, the Lorenz force was observed to affect solution flow in the bulk electrolyte, but did not influence the current/voltage characteristics of artificial pits in paramagnetic 304 stainless steel. The current/voltage characteristics of ferromagnetic iron and nickel artificial pits were affected by strong external magnetic fields, which could either enhance or suppress dissolution depending upon the field orientation. The effect was attributable to the attraction of paramagnetic ions to regions of high field gradient in the vicinity of the electrodes.

Keywords: magnetic field, artificial pit, mass transport, corrosion product, magnetic field gradient, Lorenz force.

Introduction

It is well known that magnetic fields can affect electrochemical processes by changing the mass transport of species in solution [1,2]. Mass transport is an important factor in corrosion processes, so it is of

interest to determine the extent to which magnetic fields affect corrosion, particularly of magnetic materials. A number of studies have found that magnetic fields can either accelerate or inhibit corrosion processes [3-7]. However, the mechanisms involved are not yet fully understood. They are likely to involve two forces: the Lorenz force and the field gradient force.

Lorenz Force

The effect of the Lorenz force in electrochemical systems has been observed by a number of recent researchers [5,8,9]. Its effect in a corroding system was noted as early as 1950 [10], when a droplet of electrolyte corroding a metal substrate was observed to rotate in between the poles of a magnet.

The Lorenz force acts when charge-carrying ions are moving within a magnetic field. It is the cross product of the current, ***i*** and magnetic field, **B,** as shown in Figure 1. The Lorenz force acts on the ions, which are deflected together with their solvation shells, causing fluid flow. On a disk electrode, current flows radially outwards, Figure 2. The effect of the Lorenz force is therefore to cause rotation of the solution about an axis parallel to the magnetic field. This is illustrated in Figure 3 for fields parallel and perpendicular to the electrode surface.

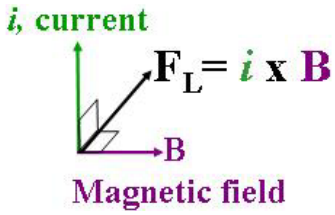

Figure 1. Schematic diagram of the Lorenz force.

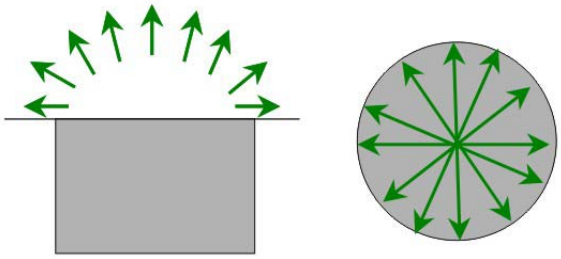

(a) (b)

Figure 2. Schematic diagram of current fluxes flowing radially outwards, (a) side view and (b) top view, from a disk electrode in an insulating plane.

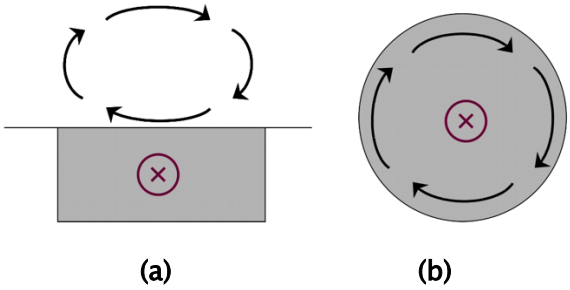

Figure 3. Schematic diagram of the effect of the Lorenz force on solution flow around a disk electrode (see Figure 2) when a magnetic field is applied (a) parallel and (b) perpendicular to the electrode surface.

Field Gradient Force

In an inhomogeneous magnetic field, paramagnetic species are attracted to the region of highest field gradient. In an electrochemical cell, this effect can be observed when a ferromagnetic electrode is magnetised in an external magnetic field. Large field gradients are created in the region adjacent to the electrode [11]. The effect is illustrated in Figure 4. Leventis *et al.* [12] theoretically proved that in the absence of convection, the field gradient causes a drift of paramagnetic species toward areas of higher field.

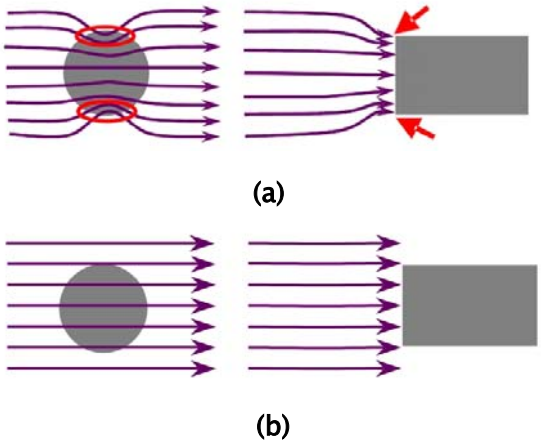

Figure 4. Schematic diagram of magnetic flux lines for (a) a ferromagnetic electrode and (b) a paramagnetic electrode in an external magnetic field. It is assumed that the electrode is a wire with a flat polished end (disk electrode), and is viewed from the end and from the side. Regions of high field gradient are indicated in red.

Pitting Corrosion and Artificial Pits

The stability of a localised corrosion site such as a pit depends upon maintaining an aggressive acidic environment inside the pit cavity that promotes metal dissolution rather than repassivation. The acidity depends upon hydrolysis of metal cations, as illustrated in Figure 5(a)

[13-18]. The pit will die (repassivate) if metal cations escape from the pit faster than they are produced by dissolution within the pit. Thus pit stability is critically dependent on mass transport of ions.

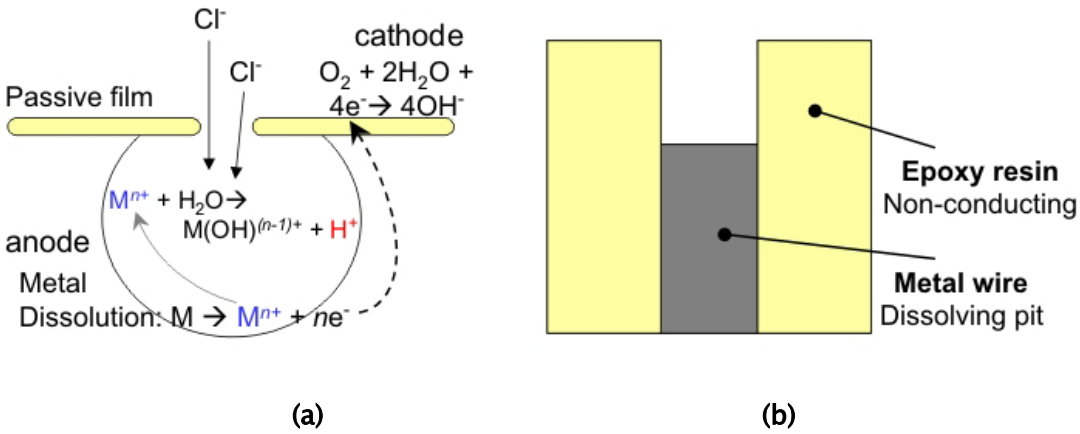

Figure 5. Schematic of (a) pits on a metal surface and, (b) 1-D artificial pit.

The effect of mass transport within pits is readily studied with a 1-D "lead in pencil" artificial pit, Figure 5(b) [13,16,18-20]. This is produced by embedding a wire in epoxy resin, and dissolving it back to produce a cavity that contains the pit solution.

Figure 6 shows the typical current/voltage characteristics of a 1-D artificial pit. The current increases linearly with voltage from **A** to **B** as the rate is controlled by the resistance in the pit cavity (Ohm's Law). When the rate of production of metal ions is faster than their diffusion out of the cavity, the region adjacent to the metal-electrolyte interface becomes supersaturated with metal ions, and a salt film layer is precipitated (**C**). There is a high potential drop across the thick layer of salt film and the curve drops to point **D** as a result. The thick salt film layer thins to its equilibrium state leading to a gradual increase in current, which reaches its steady state at point **E**. The current is then controlled by mass transport of metal ions out of the cavity, and is thus independent of potential; any increase of the potential is accommodated by the thickening of the salt film. On the reverse sweep, the salt film thins until the point at which the diffusion-limited current is equal to the ohmically-limited current for a film-free surface, **F**, when the salt film is completely dissolved. In region **G**, the ohmically-limited dissolution from a salt film-free surface is reversible.

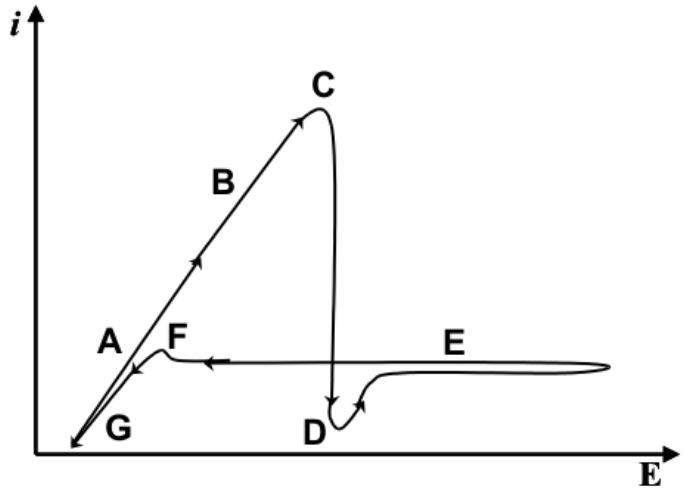

Figure 6. Current-voltage characteristics of 1-D artificial pits.

Experimental Method

Lorenz Force Observations

NdFeB disks, 10 mm in diameter, were corroded with a drop of 1 M HCl. Samples were used in the magnetised and demagnetised states. Similar disks were mounted in epoxy resin, immersed in pH 8.4 borate buffer solution, and cathodically polarised at -2 V(SCE) to produce a flow of hydrogen bubbles. 10 mm PrFeB disks, magnetised and demagnetised, were mounted in epoxy, and immersed in 1 M HNO_3 to corrode freely. Copper sheet, 2 mm thick was corroded with droplet of 40% HNO_3. An external magnetic field was applied by attaching a small NdFeB disk magnet at the back of the copper sheet. In all cases, the samples were viewed with a video camera.

1-D Artificial Pits

Iron, nickel, and 304 stainless steel wires, 0.25 mm in diameter were embedded in epoxy resin. Each wire was dissolved under potentiostatic control in 1 M NaCl to create a cavity 1 mm deep. The depth of the pit was estimated from Faraday's Law through the total charge passed during the dissolution, and the depth was confirmed with an optical microscope.

The current/voltage characteristics of the artificial pits were studied in 1 M NaCl with cyclic voltammetry at a sweep rate of 10 mV/s. In order to visualise the flow of Fe^{2+} ions in solution, 0.3% $K_3Fe(CN)_6$ was

added, which forms Prussian blue on reacting with ferrous ions. The electrochemical cell was a 1 x 1 cm cuvette. A magnetic field of 0.35 T was applied with a horseshoe magnet as shown in Figure 7.

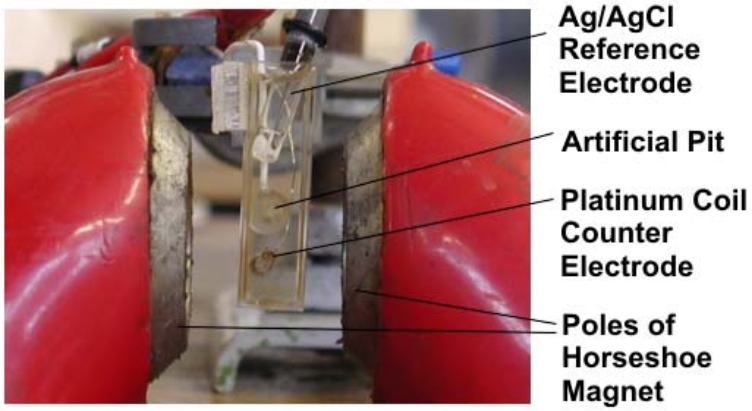

Figure 7. Experimental setup for artificial pit measurements.

Results and Discussion

NdFeB corroded vigorously in 1 M HCl, producing H_2 bubbles at the metal surface. On demagnetised NdFeB, the H_2 bubbles flowed towards the surface of the drop, as shown in Video 1. In contrast, on magnetised NdFeB, the H_2 bubbles streamed in a clockwise path in the droplet, as shown in Video 2. On the opposite face of the magnet, the stream of bubbles flows in the opposite (anticlockwise) direction, Video 3.

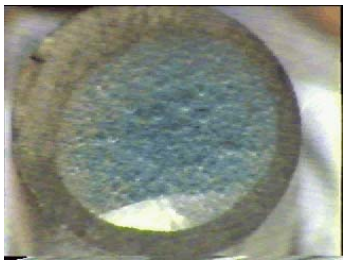

Video 1

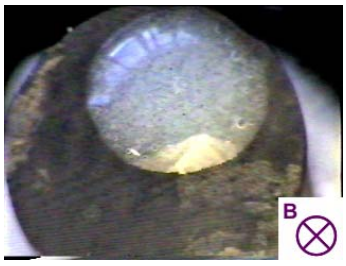

Video 2

Video 3

Videos showing the flow of H_2 bubbles produced from corrosion on Video 1: a demagnetised NdFeB; and Videos 2 and 3, opposite faces of a magnetised NdFeB disk 10 mm in diameter.

Hydrogen evolution on cathodically-polarised demagnetised NdFeB is shown in Video 4. In this case, the video camera was pointed horizontally, parallel to the flat surface of the magnet. The bubbles

flowed vertically towards the surface of the solution. On magnetised NdFeB, a helical flow of H_2 bubbles was observed, Video 5.

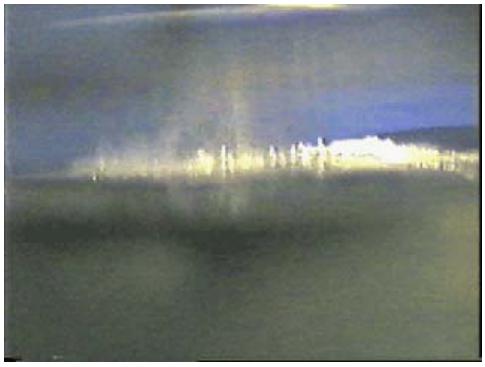

Video 4

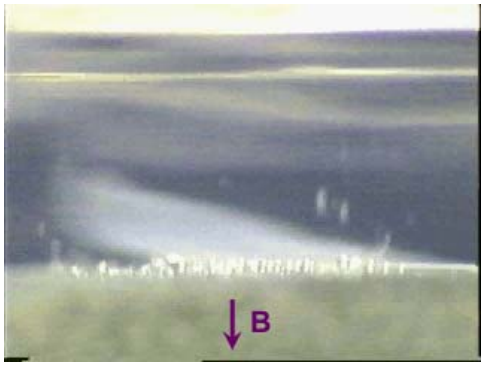

Video 5

H_2 evolution on demagnetised NdFeB (Video 4) and magnetised NdFeB (Video 5) when they were cathodically polarised.

PrFeB disks with the cross-sectional face held vertically were immersed in 1 M HNO_3. Vigorous corrosion took place with generation of bubbles. On the demagnetised sample, bubbles flowed directly upwards (Video 6), while on the magnetised sample, a rotating flow of bubbles can be seen, and a ring of dark corrosion products can be observed around the periphery of the sample (Video 7).

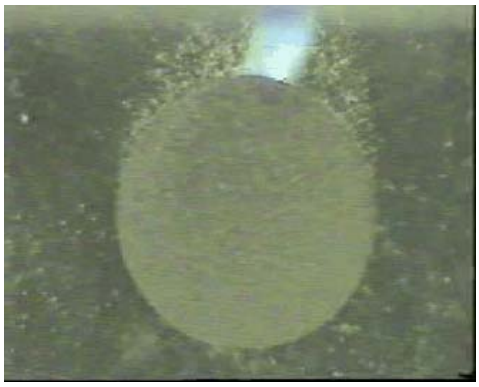

Video 6

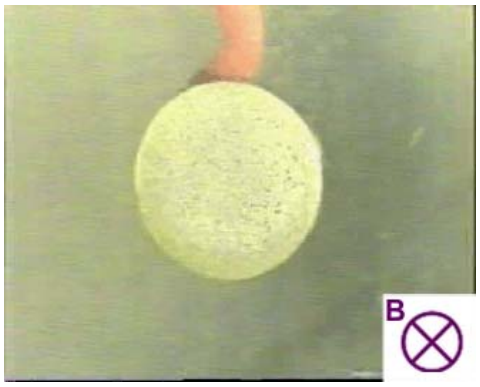

Video 7

Free corroding videos of demagnetised PrFeB (Video 6) and magnetised PrFeB (Video 7) in 1M HNO_3. Disks are 10 mm in diameter.

Copper also reacts vigorously with HNO_3. In the absence of a magnetic field, bubbles flowed directly to the surface (Video 8). When a small NdFeB magnet was attached to the back of the sheet, the bubbles were observed to flow in a circular path around the periphery of the magnet (Video 9).

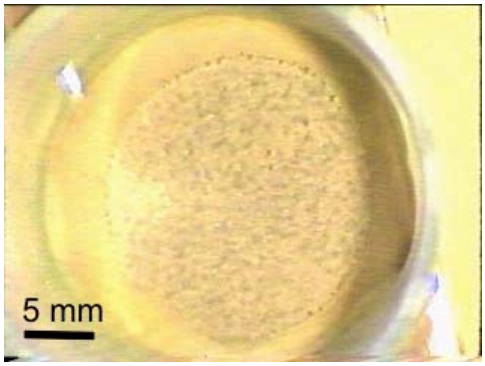

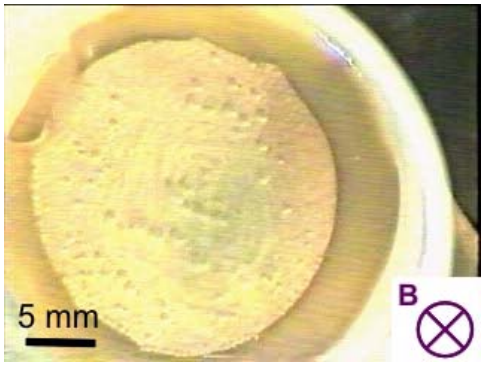

Video 8 Video 9

Cu corroding in HNO_3, Video 8 in absence of magnetic field, and Video 9 in the presence of a magnetic field

Figure 8 shows the current/voltage characteristics of an Fe artificial pit electrode. The characteristic regions shown in Figure 6 can be observed. The data from a number of sequential sweeps are shown, indicating very good reproducibility.

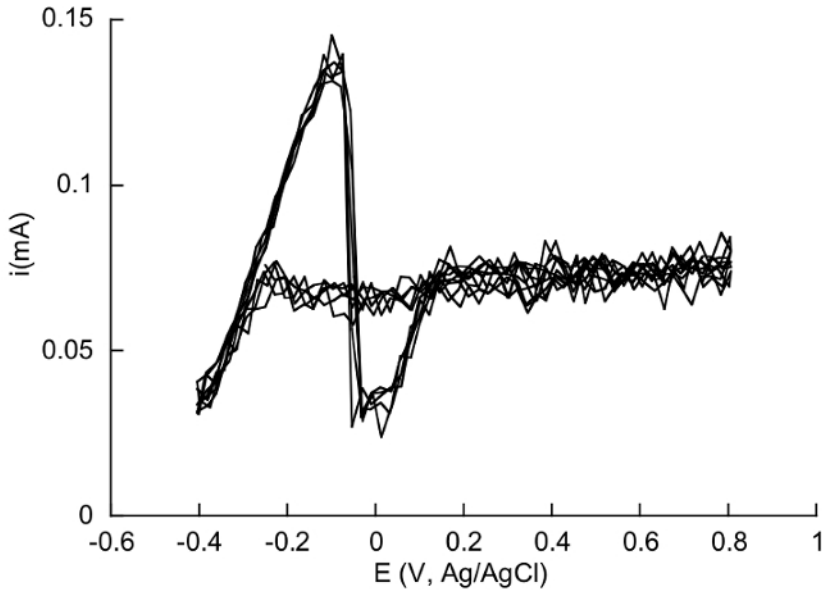

Figure 8. Current/voltage curves for an Fe artificial pit (sweep rate 10 mVs^{-1}).

Figure 9 shows an image of the Fe artificial electrode during experiment shown in Figure 8 and Video 10 shows a time-lapse video of one current/voltage cycle. During the cycle, precipitation of the salt film can be observed. It then thins (D to E in Figure 6), and thickens again as the voltage increases. It thins with decreasing voltage on the reverse sweep, and finally disappears (point G on Figure 6).

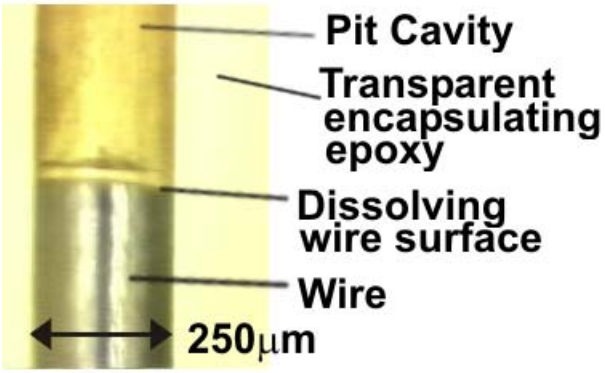

Figure 9 Artificial pit electrode.

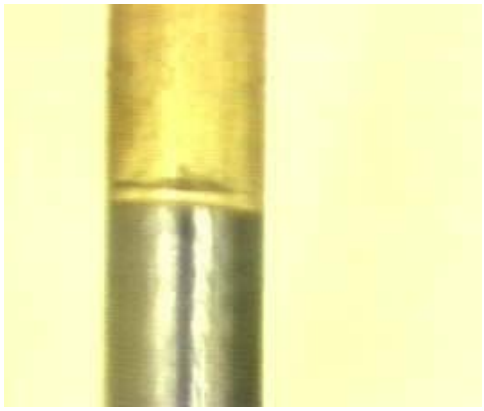

Video 10. Salt film precipitation.

An Fe artificial pit electrode was dissolved at 1 V in 1 M NaCl with added $K_3Fe(CN)_6$. In the absence of a magnetic field, the Prussian blue product streamed downwards due to the gravity, Video 11. When an external magnetic field of 0.35 T was imposed parallel to the wire (perpendicular to the pit surface), a slow vortex flow gradually developed, Video 12. When the field was imposed parallel to the pit surface (perpendicular to the wire), a more rapid vortex flow was observed, Video 13.

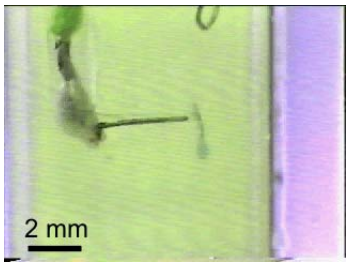

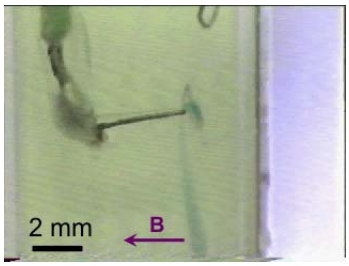

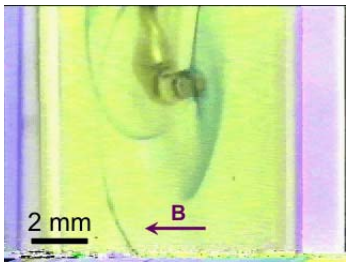

Video 11 Video 12 Video 13

Videos showing flow of Prussian blue product from an Fe artificial pit. 0.35T magnetic field parallel to the wire was present in Video 12, and perpendicular to the wire in Video 13.

The experiment was repeated with a 304 stainless steel (paramagnetic) artificial pit electrode. Figure 10 shows similar observations in the bulk solution to those for the iron electrode, confirming that the Lorenz force does not depend on the magnetic properties of electrode.

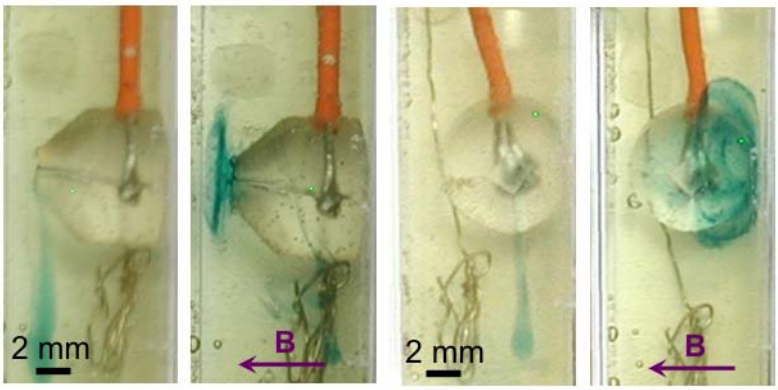

(a) (b)

Figure 10. (a) and (b) Flow of Prussian blue product from 304 stainless steel artificial pits without a magnetic field present (left) and with a 0.35 T field applied horizontally in the plane of the image (right)

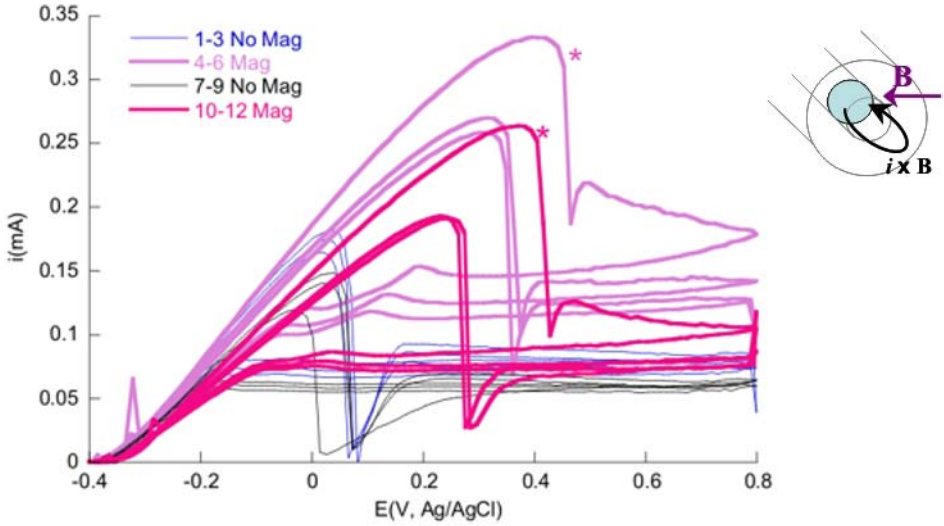

Figure 11. Current/voltage curves for a horizontal iron artificial pit (dissolving surface is vertical); a magnetic field of 0.35 T, parallel to the pit surface (perpendicular to the wire axis), was applied for cycles 4-6 and 10-12.

Figure 11 shows the current/voltage curves for an Fe artificial pit with its active dissolving surface aligned vertically (wire is horizontal). The first 3 cycles were performed in the absence of a magnetic field. A field of 0.35 T was applied just before the start of the 4th cycle. For cycles 4-6 in magnetic field, the ohmic linear region extended to a higher potential and the precipitation of salt film was delayed. The limiting current density during the diffusion-controlled process was enhanced. When the magnetic field was removed for cycles 7-9, the process reverted to the initial behaviour shown for cycles 1-3. The maximum current was enhanced again when the magnetic field was reapplied for cycles 10-12.

Attempts to observe changes within the cavity on application of a field revealed that the pit cavities sometimes contain corrosion products or gas bubbles trapped within the cavity as can be observed in Videos 14–17. In the absence of a magnetic field, no movement is observed in the interior of the pit cavity, Video 14. When a magnetic field was applied parallel to the pit surface (perpendicular to the axis of the wire), small fragments of corrosion products could be observed to flow in the cavity close to the dissolving surface. It is probably this stirring action that causes the effects observed in Figure 11.

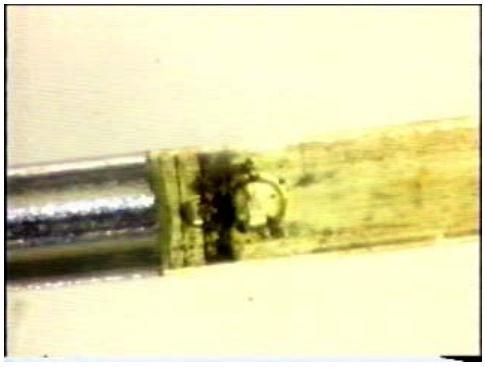

Video 14

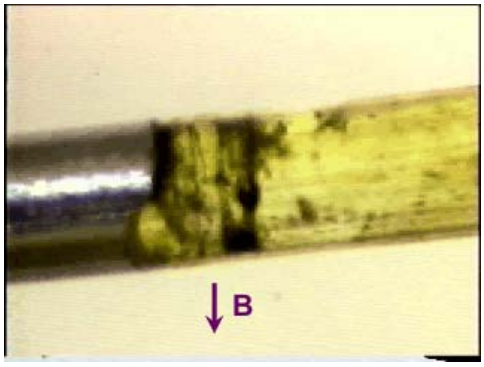

Video 15

Video sequence within the Fe artificial pit cavity (0.25 mm diameter) during constant-potential dissolution in the absence of a magnetic field, Video 14, and in the presence of a 0.35 T magnetic field, Video 15.

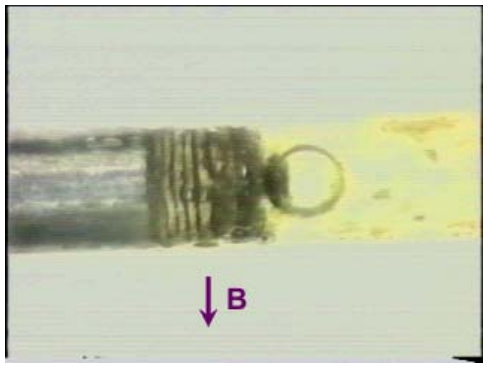

Video 16. Response of corrosion product within an Fe artificial pit cavity (0.25 mm diameter) when 0.35 T field first applied.

The loops of the very first cycle immediately after the introduction of magnetic field, marked with an asterisk* in Figure 11, are frequently larger than subsequent cycles. Video 16 shows reactions that took place on application of a magnetic field after the artificial pit had been grown for a number of cycles with no magnetic field. The corrosion products that accumulated at the pit cavity were vigorously disturbed

by the application of the magnetic field. This action created a considerably higher level of agitation than that in a stationary field and therefore the salt film precipitation was found to be more difficult after the field was first applied.

The current/voltage curves for a paramagnetic 304 stainless steel artificial pit were performed with the same magnetic field orientation. No difference was found when a magnetic field was applied, Figure 12. This suggests that the Lorenz force action found in the bulk solution (Figure 10) is not sufficient to cause changes to the current voltage characteristics. Instead, it is likely that the field gradient force causes the stirring in the cavity observed for iron (Video 15).

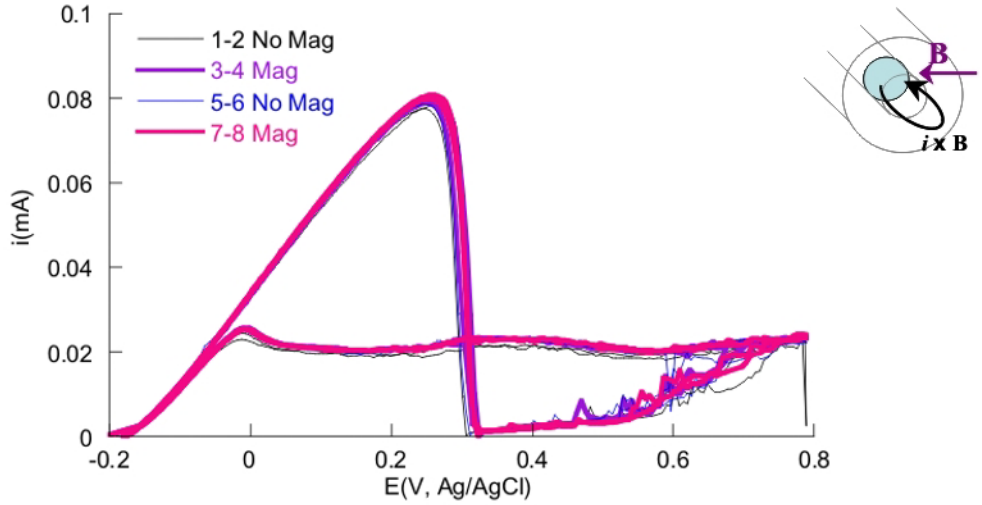

Figure 12. Current/voltage curves for a horizontal 304 stainless steel artificial pit (dissolving surface is vertical); a magnetic field of 0.35 T, parallel to the pit surface (perpendicular to the wire axis), was applied for cycles 3-4 and 7-8.

Figure 13 shows an Fe artificial pit in the same orientation (wire horizontal; dissolving surface vertical). In this case, the magnetic field was applied parallel to the wire (perpendicular to the dissolving surface). The salt film precipitation was accelerated and the limiting current suppressed. A similar experiment was performed on a ferromagnetic nickel wire (Video 17). Observation of the region close to the dissolving surface showed that on application of the field, corrosion products, presumably paramagnetic, were attracted to the periphery of the wire. This is the region of highest field gradient, as shown in Figure 14. This suggests that the enhanced formation of a salt film and suppression of diffusion in the cavity shown in Figure 13

are caused by the field gradient effect, which attracts the paramagnetic ions and corrosion products to the dissolving surface, (particularly the periphery), enhancing salt film formation and decreasing the rate of diffusion.

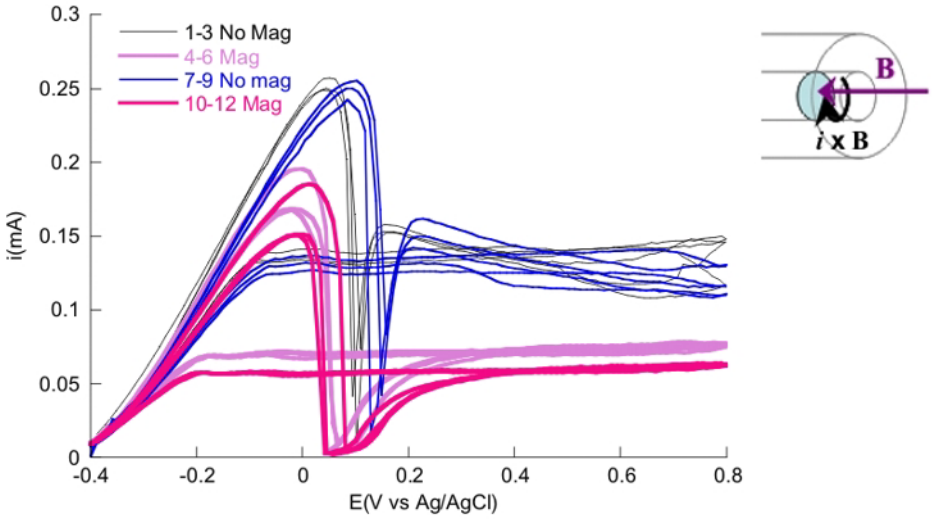

Figure 13. Current/voltage characteristics of an Fe pit, vertical pit surface (horizontal wire) with a magnetic field applied parallel to the wire (perpendicular to the pit surface) for cycles 4-6 and 10-12.

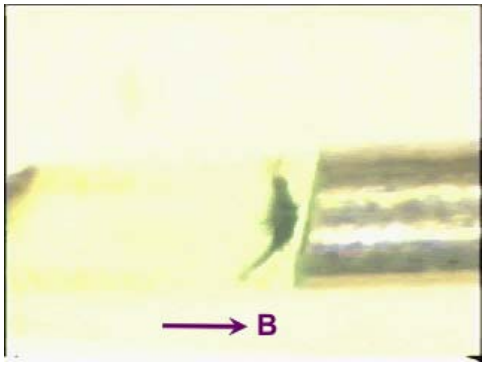

Video 17

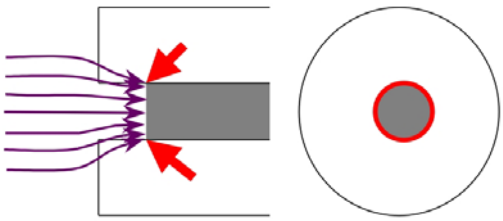

Figure 14

Video 17. Ni artificial pit (0.25 mm diameter), paramagnetic species were attracted to the highest field gradient region when the magnetic field was first applied.

Figure 14. Schematic diagram showing the field gradient around a paramagnetic wire electrode in an external magnetic field: high field gradient regions are shown in red.

This was confirmed by removing the wires after the experiments and observing them with the scanning electron microscope. A wire that had dissolved in the absence of the field was slightly concave (Figure 15(a)). When the field was applied perpendicular to the wire (parallel to the dissolving surface), the surface appeared similar (Figure 15(b)). However, when the field was applied parallel to the wire (perpendicular

to the surface), the surface was deeply convex Figure 15(c), supporting the idea that paramagnetic ions and corrosion products had been attracted to the periphery of the wire (the position of highest field gradient), suppressing dissolution.

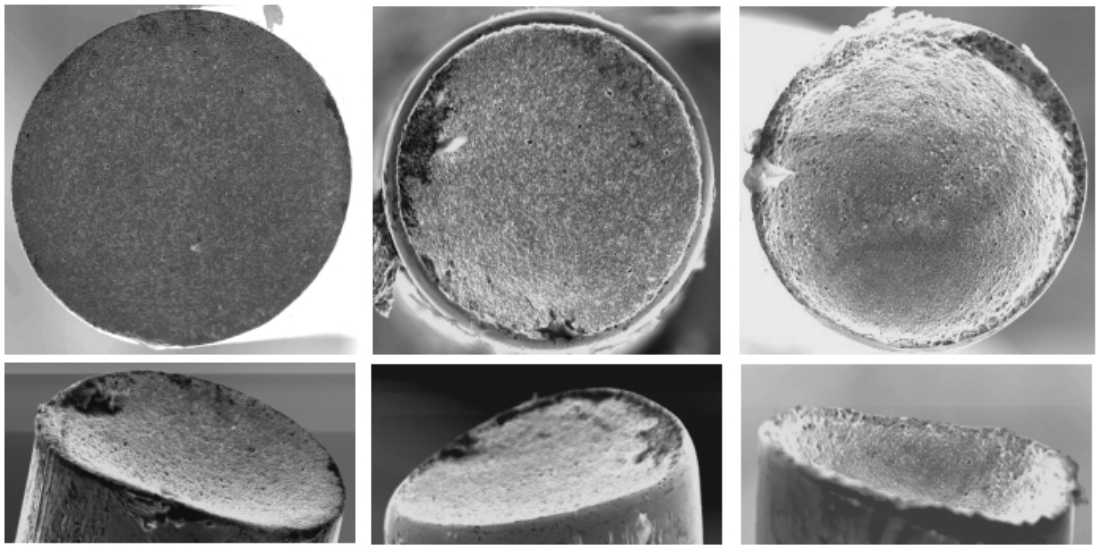

(a) (b) (c)

Figure 15. Surface of artificial pits (0.25 mm diameter) after dissolution in (a) no magnetic field, (b) a magnetic field perpendicular to the wire (parallel to the surface), and (c) a magnetic field parallel to the wire (perpendicular to the surface). The upper panel shows a top view and bottom panel shows a side view.

Conclusions

The results show that the presence of a magnetic field can either enhance or suppress corrosion reactions through their effect on mass transport. Both the Lorenz force and field gradient effects can play a role, but relatively large magnetic fields are required. In the case of artificial pits, the field gradient effect rather than the Lorenz force was important. Thus, effects of this magnitude are unlikely to be observed for real pits where the local field gradients are likely to be far lower.

Acknowledgements

This work is supported by UUK (ORS award for YC Tang) and the University of Birmingham. The authors would also like to thank the Applied Alloy Chemistry Group for provision of magnets. Helpful discussions with Prof Nick Leventis are gratefully acknowledged.

References

1. T. Z. Fahidy, 'Reviews of Applied Electrochemistry 8. Magnetoelectrolysis', *Journal of Applied Electrochemistry*, **13**, 5, pp553-563, (1983).

2. O. Aaboubi, J. P. Chopart, J. Douglade, A. Olivier, C. Gabrielli and B. Tribollet, 'Magnetic-Field Effects on Mass-Transport', *Journal of the Electrochemical Society*, **137**, 6, pp1796-1804, (1990).

3. A. Chiba, K. Kawazu, O. Nakano, T. Tamura, S. Yoshihara and E. Sato, 'The Effects of Magnetic-Fields on the Corrosion of Aluminum Foil in Sodium-Chloride Solutions', *Corrosion Science*, **36**, 3, pp539-543, (1994).

4. I. Leshev, M. Mitov and T. Peev, 'Magnetic field effect on steel corrosion', International Corrosion Conference, 2002.

5. R. Aogaki and M. Asanuma, 'Magnetic Field Effect on Metal Corrosion', 1st International Symposium on New Magneto-science, 1999.

6. A. Rucinskiene, G. Bikulcius, L. Gudaviciute and E. Juzeliunas, 'Magnetic field effect on stainless steel corrosion in FeCl3 solution', *Electrochemistry Communications*, **4**, 1, pp86-91, (2002).

7. K. Shinohara and R. Aogaki, 'Magnetic field effect on copper corrosion in nitric acid', *Electrochemistry*, **67**, 2, pp126-131, (1999).

8. K. M. Grant, J. W. Hemmert and H. S. White, 'Magnetic focusing of redox molecules at ferromagnetic microelectrodes', *Electrochemistry Communications*, **1**, 8, pp319-323, (1999).

9. K. M. Grant, J. W. Hemmert and H. S. White, 'Magnetic field driven convective transport at inlaid disk microelectrodes - The dependence of flow patterns on electrode radius', *Journal of Electroanalytical Chemistry*, **500**, 1-2, pp95-99, (2001).

10. F. Blaha, 'Use of a magnetic field in detecting corrosion currents', *Nature*, 4223, pp607, (1950).

11. M. D. Pullins, K. M. Grant and H. S. White, 'Microscale confinement of paramagnetic molecules in magnetic field gradients surrounding ferromagnetic microelectrodes', *Journal of Physical Chemistry B*, **105**, 37, pp8989-8994, (2001).

12. N. Leventis and X. R. Gao, 'Magnetohydrodynamic electrochemistry in the field of Nd-Fe-B magnets. Theory, experiment, and application in self-powered flow delivery systems', *Analytical Chemistry*, **73**, 16, pp3981-3992, (2001).

13. G. T. Gaudet, W. T. Mo, T. A. Hatton, J. W. Tester, J. Tilly, H. S. Isaacs and R. C. Newman, 'Mass-Transfer and Electrochemical Kinetic Interactions in Localized Pitting Corrosion', *AIChE Journal*, **32**, 6, pp949-958, (1986).

14. M. Kaneko and H. S. Isaacs, 'Effects of molybdenum on the pitting of ferritic- and austenitic-stainless steels in bromide and chloride solutions', *Corrosion Science*, **44**, 8, pp1825-1834, (2002).

15. M. Kaneko and H. S. Isaacs, 'Pitting of stainless steel in bromide, chloride and bromide/chloride solutions', *Corrosion Science*, **42**, 1, pp67-78, (2000).

16. U. Steinsmo and H. S. Isaacs, 'Dissolution and Repassivation Kinetics of Fe-Cr Alloys in Pit Solutions .1. Effect of the Surface Salt Layer', *Journal of the Electrochemical Society*, **140**, 3, pp643-653, (1993).

17. G. S. Frankel, 'Pitting corrosion of metals - A review of the critical factors', *Journal of the Electrochemical Society*, **145**, 6, pp2186-2198, (1998).

18. N. J. Laycock and R. C. Newman, 'Localised dissolution kinetics, salt films and pitting potentials', *Corrosion Science*, **39**, 10-11, pp1771-1790, (1997).

19. H. S. Isaacs, 'The behaviour of resistive layer in the localised corrosion of stainless steel', *Journal of the Electrochemical Society*, **120**, 11, pp1456-1462, (1973).

20. J. W. Tester and H. S. Isaacs, 'Diffusional effect in simulated localised corrosion', *Journal of the Electrochemical Society*, **122**, 11, pp1438-1445, (1975).